J. Iron Steel Res. Int. (2018) 25:830–838
https://doi.org/10.1007/s42243-018-0116-1

ORIGINAL PAPER

Microstructure and mechanical behavior of a low-density Fe–12Mn–9Al–1.2C steel prepared using centrifugal casting under near-rapid solidification

Wei He[1] · Bi-lei Wang[1] · Yang Yang[1] · Yun-hu Zhang[1] · Lian Duan[1] · Zhi-ping Luo[2] · Chang-jiang Song[1] · Qi-jie Zhai[1]

Received: 23 August 2017 / Revised: 4 November 2017 / Accepted: 27 November 2017 / Published online: 1 August 2018

Abstract
It is vital for emission reduction and energy saving to lighten the weight of automobile. Low-density Fe–Mn–Al–C steels with high strength and excellent ductility have become a promising type of material in the automotive industry. Thus, a new approach was proposed by using centrifugal casting to produce the low-density Fe–12Mn–9Al–1.2C steel with high performance under near-rapid solidification in a near-net shape. The produced steel strips, with a thickness of 2.5 mm and a density of 6.89 g/cm^3, were examined for their microstructures and mechanical properties. The results showed that mechanical properties of as-cast steel strip reached 1182 MPa in ultimate tensile strength and 28.1% in total elongation. Aging treatment at 400 or 600 °C for 3 h enhanced tensile strength of the steel strips, while aging at 800 °C dramatically decreased its elongation. Moreover, Young's modulus of the steel strip improved with the increment of aging temperature. The relationship between the mechanical properties and the microstructures was discussed. The results demonstrated that advanced low-density steels with promising mechanical properties could be directly produced from liquid by this simple process.

Keywords Low-density steel · Near-net shape · Mechanical property · Microstructure · Near-rapid solidification

1 Introduction

Weight lightening of automotive components is a major way to reduce the greenhouse gas emission and improve fuel efficiency in the automotive industry [1–4]. To decrease vehicle weight, there are several approaches from the perspective of materials: reducing the density of steel, reducing the amount of steels by enhancing the strength of steel, or increasing applications of lightweight alloys such as titanium, aluminum or magnesium alloys. However, it is unsustainable to decrease the thickness of car components unlimitedly through enhancing the strength of steel, because the weight lightening based on gauge reduction will remarkably reduce the stiffness of the parts [5]. Moreover, the high cost of lightweight alloys is a noticeable disadvantage for cost-effective automobile components [6].

The Fe–Mn–Al–C steel was recently reappraised as the promising automobile steel on account of its low density, high strength and excellent ductility [7, 8]. Significant reduction of density by 10–20% in a low-density Fe–Mn–Al–C steel is the great advantage in lightening of automotive components, which makes its specific strength more appealing against lightweight alloys because of the cost [9]. Furthermore, the addition of Al in steels could improve the capability of resisting hydrogen-associated failure and oxidation to some extent [10]. It has been widely found that the deformation mechanisms such as transformation-induced plasticity, twinning-induced plasticity and dislocation slip are helpful to improve the strength and ductility, which is typically characterized by a high product of

✉ Chang-jiang Song
riversong@shu.edu.cn; riversxiao@163.com

[1] State Key Laboratory of Advanced Special Steel, Shanghai Key Laboratory of Advanced Ferrometallurgy, School of Materials Science and Engineering, Shanghai University, Shanghai 200444, China

[2] Department of Chemistry and Physics, Fayetteville State University, Fayetteville, NC 28301, USA

ultimate tensile strength and total elongation for 30–70 GPa % [11–16].

However, the traditional production process of the low-density Fe–Mn–Al–C steel not only consumes a lot of energy due to the repeated heating and cooling but also produces several problems in the procedures. First of all, the high contents of Mn and Al usually result in casting cracks, and severe edge cracks could appear during hot/cold rolling because of the high deformation resistance of the steel [17]. Secondly, oxidation at high temperatures is an evident issue during the annealing and hot rolling process [7].

A potential approach to fabricate the advanced low-density steel is using a near-net shape method under near-rapid solidification. The near-net shape production would clearly reduce the energy consumption during the rolling deformation. The near-rapidly solidified material possesses features of ultrafine microstructure, low segregation, high solid solution and possibly non-equilibrium or metastable phases [18–22]. In the traditional process route, the homogenization treatment is conducted to decrease the segregation of alloying element, and grain refinement is achieved during the hot/cold rolling process. The quenching procedure is to promote the formation of non-equilibrium phases like martensite, metastable austenite, and nano-scale particles and to expand the solid solubility limit of alloying elements. It has been proved by previous studies [23–25] that the Fe–Mn-based steels directly fabricated from liquid by near-rapid solidification possess satisfactory mechanical properties, even better than those obtained from the traditional process.

In this work, a near-net shape method under near-rapid solidification was used to produce the low-density Fe–12Mn–9Al–1.2C steel. And, the effects of aging treatment on the mechanical properties and structures were investigated.

2 Experimental

The experimental material is Fe–12Mn–9Al–1.2C (wt%) steel. The material was prepared from high purity Fe (99.99%), Mn (99.9%), Al (99.9%) and C (99.8%). The traditional production route of low-density Fe–Mn–Al–C steels is schematically shown in Fig. 1 [26–29]. The solidified ingots usually required homogenization treatment at a high temperature (about 1200 °C) for 2–4 h. Then, they were hot rolled and cold rolled to produce approximately 1 mm thick sheet. The subsequent annealing treatments were performed between 500 and 1000 °C for several hours and then quenched into water.

In present work, centrifugal casting was used to produce the low-density steels in a near-net shape. It was a customer-designed method to produce larger size thin strips under near-rapid solidification, different from the injection casting or suction casting [25]. The setup of the centrifugal casting is illustrated in Fig. 2. The whole production process was conducted as follows. The cylindrical cavity was vacuumed and then filled with high purity argon. The sample was heated to melt by induction coils. After the rotary platform reached a given speed of 600 r/min steadily, moveable baffle was manually drawn out. Finally, the molten metal flowed into the rotary copper mold through a graphitic funnel and solidified within a short period of time (the calculated cooling rate is about 5×10^3 K/s [30]). A thin strip with size of (70–90) mm × 60 mm × 2.5 mm was obtained. Then, the steel strip was divided into two parts along the central line in thickness direction. Both parts were mechanically polished to 1 mm in thickness for mechanical property test. In addition, microstructure observation was carried out in position of 500–600 μm beneath the surface.

The composition of the steel strip was Mn 11.75, Al 9.12, C 1.23, and Fe balance (all in wt%), measured by inductively coupled plasma-optical emission spectrometer (PERKINE 7300DV) and carbon–sulfur analyzer (CS

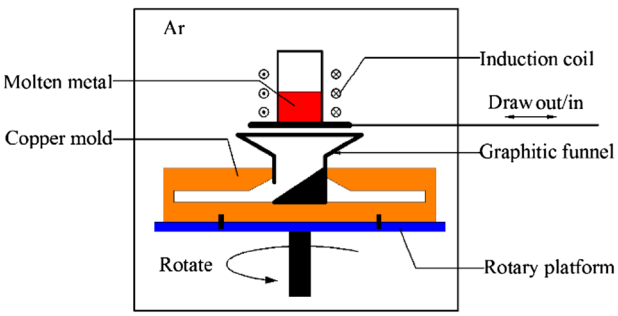

Fig. 2 Schematic setup of centrifugal casting

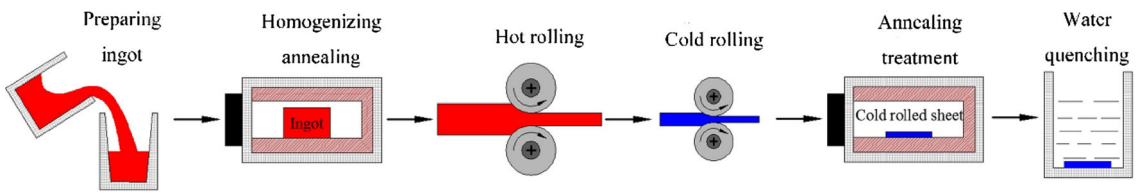

Fig. 1 Production route of low-density steel reported in the studies [26–29]

600CR). Archimedes' principle–gas expansion displacement method was adopted to measure the density of the steel strip (ACCUPYC II 1340 density analyzer). The measured density of the steel was about 6.89 g/cm^3, which decreased by 12.34% compared with ferrite. Some strips were heated to 400, 600 and 800 °C within 3 h, and aged for 3 h inside a tubular vacuum furnace (10^{-4} Pa vacuum), then cooled to room temperature.

Microstructure was characterized using an optical microscope (OM, Zeiss Axio Imager A2 m) and a scanning electron microscope (SEM, Phenom ProX). Samples for OM and SEM observations were mechanically polished and then etched by a solution containing 3.3 vol.% nitric acid, 3.3 vol.% acetic acid and 0.1 vol.% hydrofluoric acid. For observation with a transmission electron microscope (TEM, JEM-2100F operated at 200 kV), samples were electrolytically thinned by a twin-jet polisher in a solution of 10 vol.% perchloric acid at temperature of − 30 °C at 30 V. The constituent phases were identified using an X-ray diffractometer (XRD, D/Max-2200, Cu target, operated at 40 kV and 40 mA) with a scan rate of 4 (°)/min, and the volume fraction of ferrite phases was determined by a ferrite instrument (FERITSCOPE FMP30).

Young's modulus of the specimens was tested by three points bending method (NETZSCH-TMA402), and the gauge section is 22 mm × 2 mm × 0.7 mm. Two specimens were prepared for each condition, and each specimen was measured by two times, giving four measurement data for each steel strip. Tensile tests were performed up to failure using an MTS Criterion Model 44 tensile testing facility with a 12-mm gauge extensometer at room temperature, with strain rate of 2.5×10^{-4} s^{-1}. The tensile specimens contained gauge section of 20 mm × 4 mm × 1 mm, and their surfaces were mechanically polished. Moreover, four samples were tested for the tensile test of each steel strip.

3 Results and discussion

3.1 Microstructure

Figure 3 shows OM images of as-cast, and 400, 600, and 800 °C-aged steel strips. In all strips except the one aged at 800 °C, irregular short rod or granular ferrites are uniformly embedded in austenite matrix, while in the low-

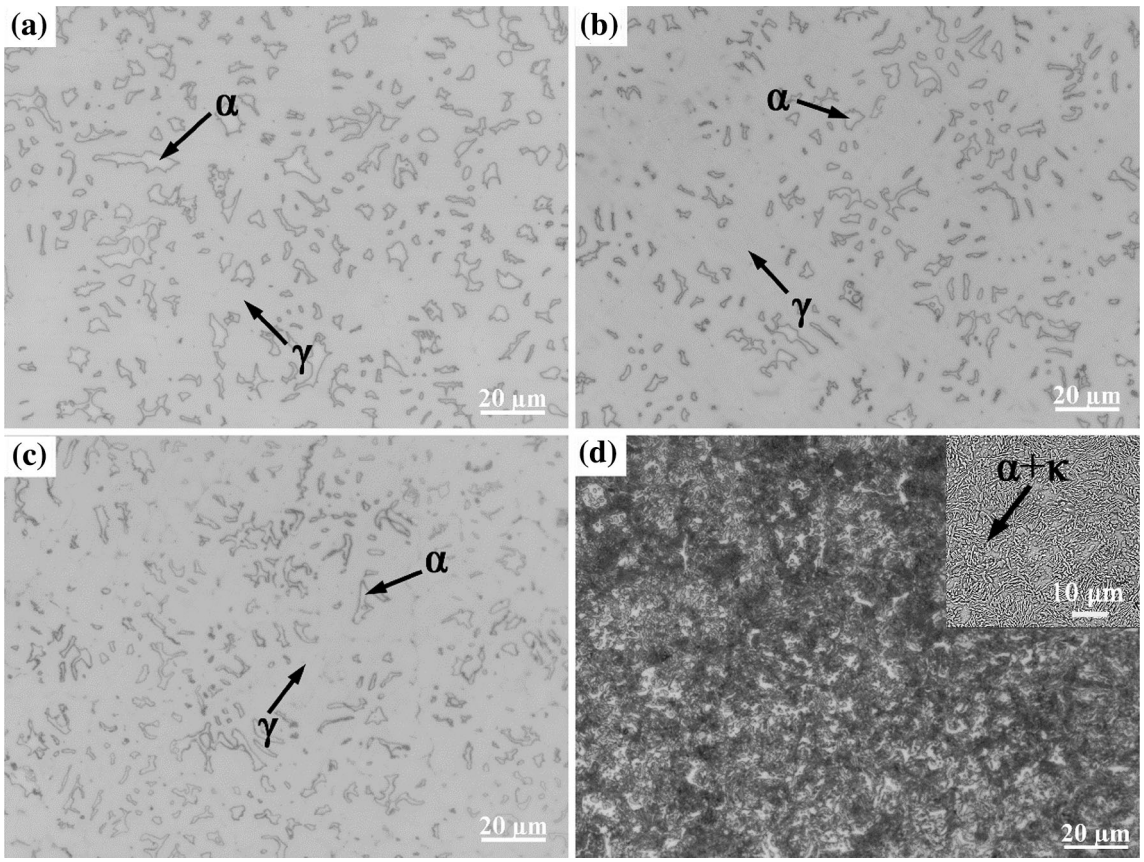

Fig. 3 Optical images of steel strips. **a** As-cast; **b** aged at 400 °C; **c** aged at 600 °C; **d** aged at 800 °C. Inset in (**d**) is an SEM image

density steel with the similar compositions made by traditional method, ferrites are banded [31, 32]. Aging treatment at 400 or 600 °C for 3 h does not evidently change the microstructure of these steel strips, although the ferrites fraction is slightly increased, as shown in Fig. 3c. However, after aging at 800 °C, irregular short rod or granular ferrite disappears, which is replaced with dispersed fine microstructure, as shown in Fig. 3d. SEM observation in a higher magnification reveals dense lamellar microstructure, as shown in the inset of Fig. 3d.

From XRD results as shown in Fig. 4, austenite is the major constituent phase in the as-cast, and 400 and 600 °C-aged steel strips. There are only two weak diffraction peaks of α-ferrite phase at 42.5° and 80.9°, respectively, in these three samples. No reflections from κ-carbide are present. However, in the 800 °C-aged steel strip, reflections from austenite phase disappear; instead, α phase becomes the major constituent phase, along with the κ-carbide. These results are consistent with the observation in Fig. 3d.

Table 1 lists the ferrite volume fractions of the four steel strips. The ferrite fraction increases with the aging treatment temperature.

3.2 Mechanical properties

Figure 5 shows the tensile properties of the four steel strips. From the engineering stress–strain curves, ultimate tensile strength (UTS) and total elongation (TE) of the as-cast steel strip are determined as 1182 MPa and 28.1%, respectively. Aging treatment at 400 and 600 °C increases the UTS to 1266 and 1393 MPa, respectively, while their TE first increases to 30.7% and then decreases to 12.6%. However, for the steel strip aged at 800 °C, both the strength and elongation sharply decrease to 1092 MPa and 0.6%, respectively, because of the appearance of dense coarse κ-carbides. The product of UTS and TE of the 400 °C-aged steel strip reaches 38.9 GPa %, which is the best comprehensive mechanical property in these four steel strips.

Figure 6 shows the true stress-true strain and strain hardening rate (SHR) curves of the as-cast, 400 and 600 °C-aged steel strips. All these three steel strips possess a very high initial SHR at approximately 4500 MPa, which

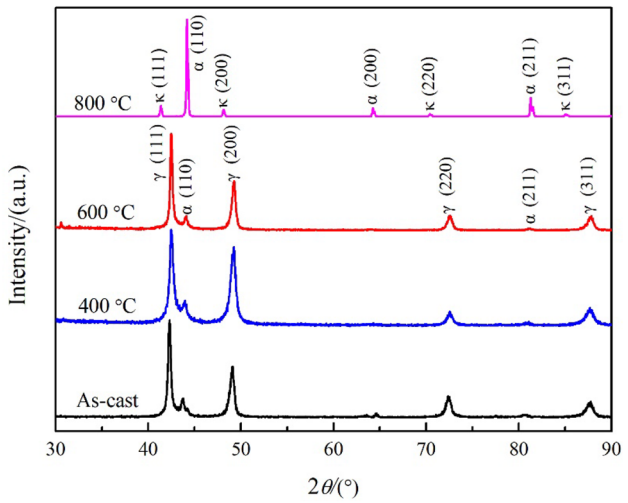

Fig. 4 XRD profiles of as-cast and aged steel strips

Table 1 Ferrite volume fractions of as-cast and aged Fe–12Mn–9Al–1.2C steel strips

Specimen	As-cast	400 °C	600 °C	800 °C
Ferrite fraction/vol.%	13.3	14.6	22.7	78.6

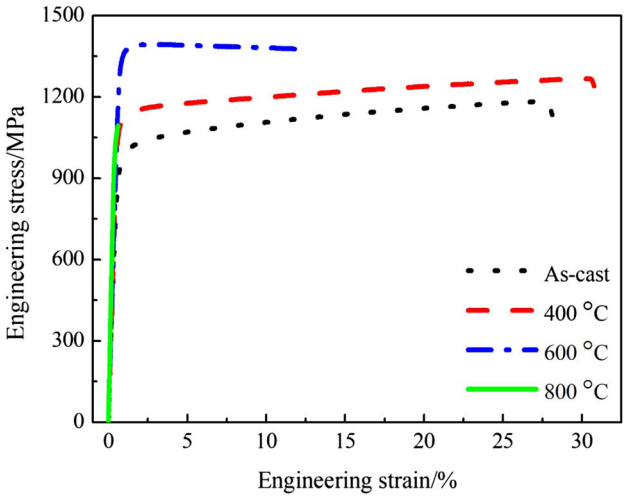

Fig. 5 Tensile properties of as-cast and aged steel strips

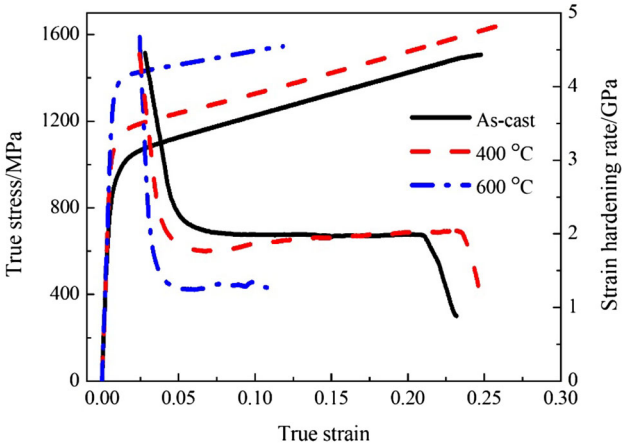

Fig. 6 True stress-true strain and strain hardening rate curves of as-cast and aged steel strips

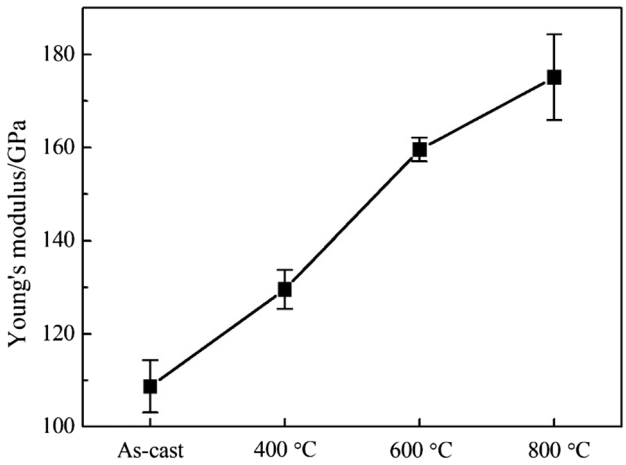

Fig. 7 Influence of aging temperature on Young's modulus of steel strip

decreases drastically until the true strain attains 0.05 in the first strain stage. In the second strain stage, the as-cast steel strip maintains a constant SHR level around 2000 MPa, and the 400 °C-aged steel strip exhibits an increased SHR from 1764 to 2042 MPa with the increase in the strain, while SHR of the 600 °C-aged steel strip is only 1312 MPa. In the third strain stage, starting from 0.23 and 0.25, respectively, the SHRs of the as-cast and 400 °C-aged steel strips decrease rapidly until fracture. The steel strip aged at 600 °C does not exhibit the third stage clearly.

Figure 7 shows the Young's modulus of the four steel strips. The Young's modulus is improved by 19.2, 46.8 and 61.1% after the aging treatment at 400, 600 and 800 °C, respectively, compared with as-cast steel strip. The aging treatment effectively improves the Young's modulus of the steel strips.

3.3 TEM analysis

To investigate the changes of mechanical properties by aging treatment, TEM analysis was carried out. TEM images of as-cast steel are shown in Fig. 8. In the bright field (BF) image in Fig. 8a, a piece of ferrite inserts into the austenite matrix, as confirmed by selected-area diffraction pattern (SADP) in Fig. 8c. Figure 8b shows a BF image of the austenite matrix, where the circled area is selected for electron diffraction, as shown in Fig. 8d. A set of weak superlattice reflections (marked with green arrows) are observed, which are from the precipitation of $(Fe,Mn)_3AlC_x$ type κ-carbides with $L'1_2$ structure [33]. However, the content of κ-carbide is too low to be detected clearly in XRD (Fig. 4). In the high-resolution TEM images in Fig. 8e, f, crystalline planes of κ-carbide marked with κ are visible, with lattice spacing twice as that of the austenitic matrix. The size of κ-carbide is approximately 5–10 nm.

Figure 9 shows the TEM analysis of 600 °C-aged steel strip. Some lamellae containing α-ferrite and κ-carbide appear, as shown in Fig. 9a. Figure 9b shows a magnified image of the lamellar microstructure, showing the width of κ-carbide in 20–50 nm. The SADPs in Fig. 9c, d confirm the α and κ phases. Thus, a eutectoid transformation of $\gamma \rightarrow \alpha + \kappa$ occurred partially in austenite during 600 °C aging treatment. In Fig. 9e, an isolate ferrite appears in the austenite matrix, which is similar to the microstructure observed in the as-cast steel strip. Moreover, larger island κ-carbide is also observed, as shown in Fig. 9f, and its elemental composition is determined as Fe 58.37, Mn 12.94, Al 13.34 and C 15.35 (all in wt%) by EDS.

It can be concluded that aging treatment increases the fractions of ferrite and κ-carbides since the metastable austenite of the near-rapidly solidified steel strip transforms into the ferrite and κ-carbides. As Dalai et al. [34] found that an incorporation of 10 vol.% TiC particle in austenitic manganese steel could boost the increase in elastic modulus, and it could be speculated that the increase in strength and Young's modulus after aging at 400 and 600 °C was attributed to increased nano-size κ-carbides. Moreover, the Young's modulus (210 GPa) of pure ferrite is also slightly higher than that of pure austenite (195 GPa) [34]. Increasing the ferrite fraction is beneficial to improve both strength and Young's modulus.

3.4 Comparison with steels prepared by traditional method

Table 2 lists a comparison of investigated strips with several other Fe–Mn–Al–C steels prepared by traditional methods. Compared with the low-density steels with similar composition made by the traditional methods, the present Fe–12Mn–9Al–1.2C steel strip solidified under near-rapid solidification contains a higher fraction of austenite phase. The ferrite is in irregular short rod or granular shape with smaller size, while in steels made by traditional methods, ferrites are banded [31, 32]. These microstructural features favor the mechanical properties. Moreover, nano-scale κ-carbides appear in the austenite matrix in the present sample, which contributes to the higher tensile strength. As a result, mechanical properties of as-cast steel strip are similar to or even better than those produced by the traditional methods.

The improved strength and Young's modulus of strips after aging treatment at 400 and 600 °C are mainly attributed to more precipitation of κ-carbides and slight increase in ferrite fraction. The improved ductility after 400 °C aging treatment was probably related to the release of thermal stress and the decrease in dislocation density of the steel strip caused by rapid cooling rate [25]. In addition, the specific strength of the steel strip prepared under near-

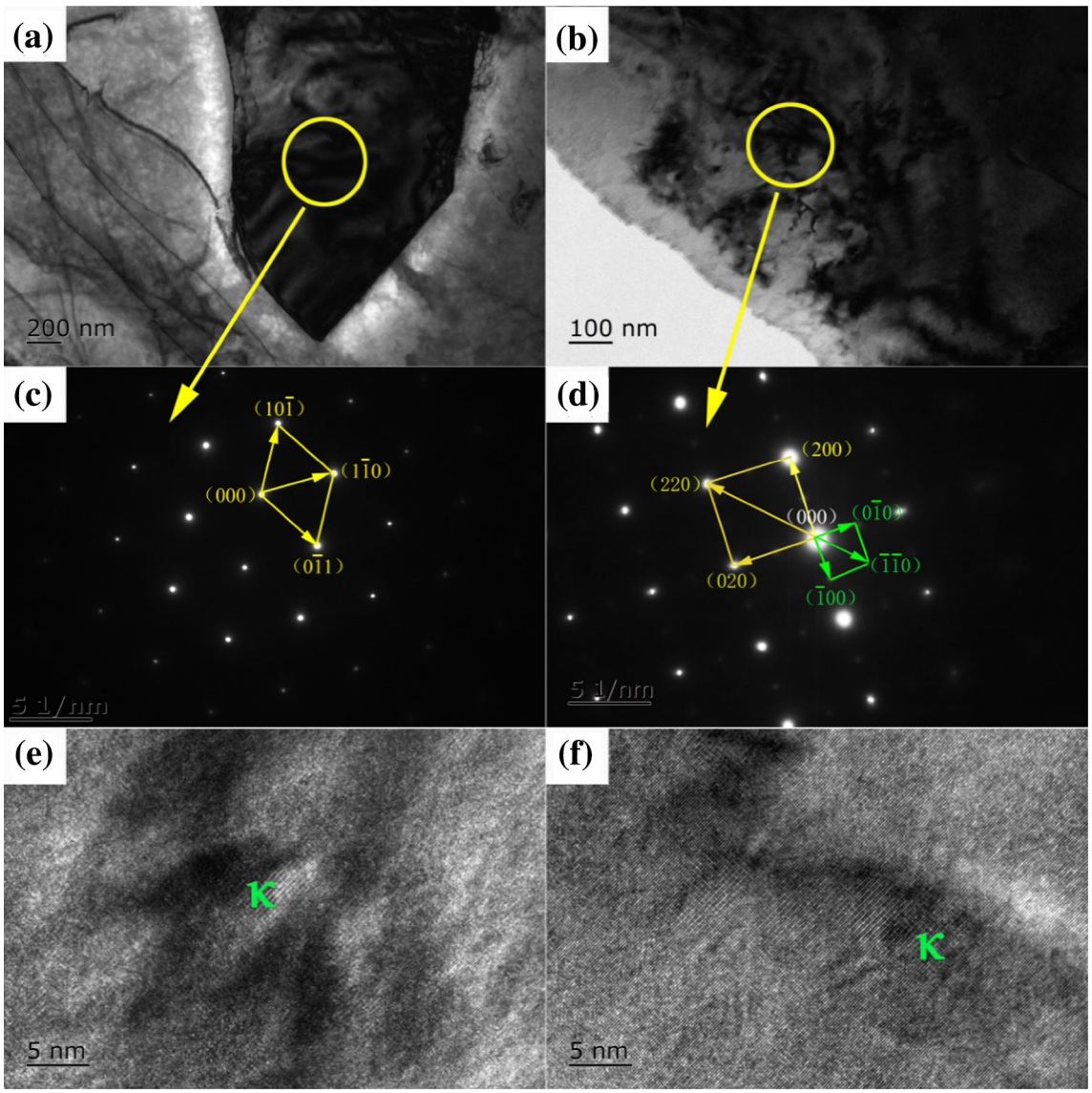

Fig. 8 TEM images of as-cast steel strip. **a** BF image of ferrite in austenite matrix; **b** BF image of austenite with κ-carbide; **c** SADP taken from circled area in (**a**), along $[111]_{\alpha}$ zone axis of ferrite; **d** SADP taken from circled area in (**b**), along $[001]_{\gamma}//[001]_{\kappa}$ zone axes; **e**, **f** high-resolution images of κ-carbides in austenitic matrix

rapid solidification is much higher than that of the low-density steels with similar composition made by the traditional methods, and the specific strength of 600 °C-aged steel strip is even more than 200 MPa cm^3/g, which is far higher than those of low-density steels made by traditional methods.

The mechanical properties of low-density steels and lightweight alloys are compared in Fig. 10, according to the studies [26, 32, 35–46]. Titanium alloy has the best specific strength, but its plasticity is limited on account of the fact that the elongation is usually lower than 15%. Compared with magnesium and aluminum alloys, low-density steel possesses comparable specific strength while better plasticity. Considering the comprehensive mechanical property and cost, the low-density steel would have great potential applications in weight lightening of automobiles.

It can be concluded that the near-net shape method under near-rapid solidification condition can directly produce advanced high strength and low-density Fe–Mn–Al–C steel from liquid. It may become an alternative way to produce low-density steels due to its simplified process, along with other advantages such as energy saving, high efficiency and benign environment.

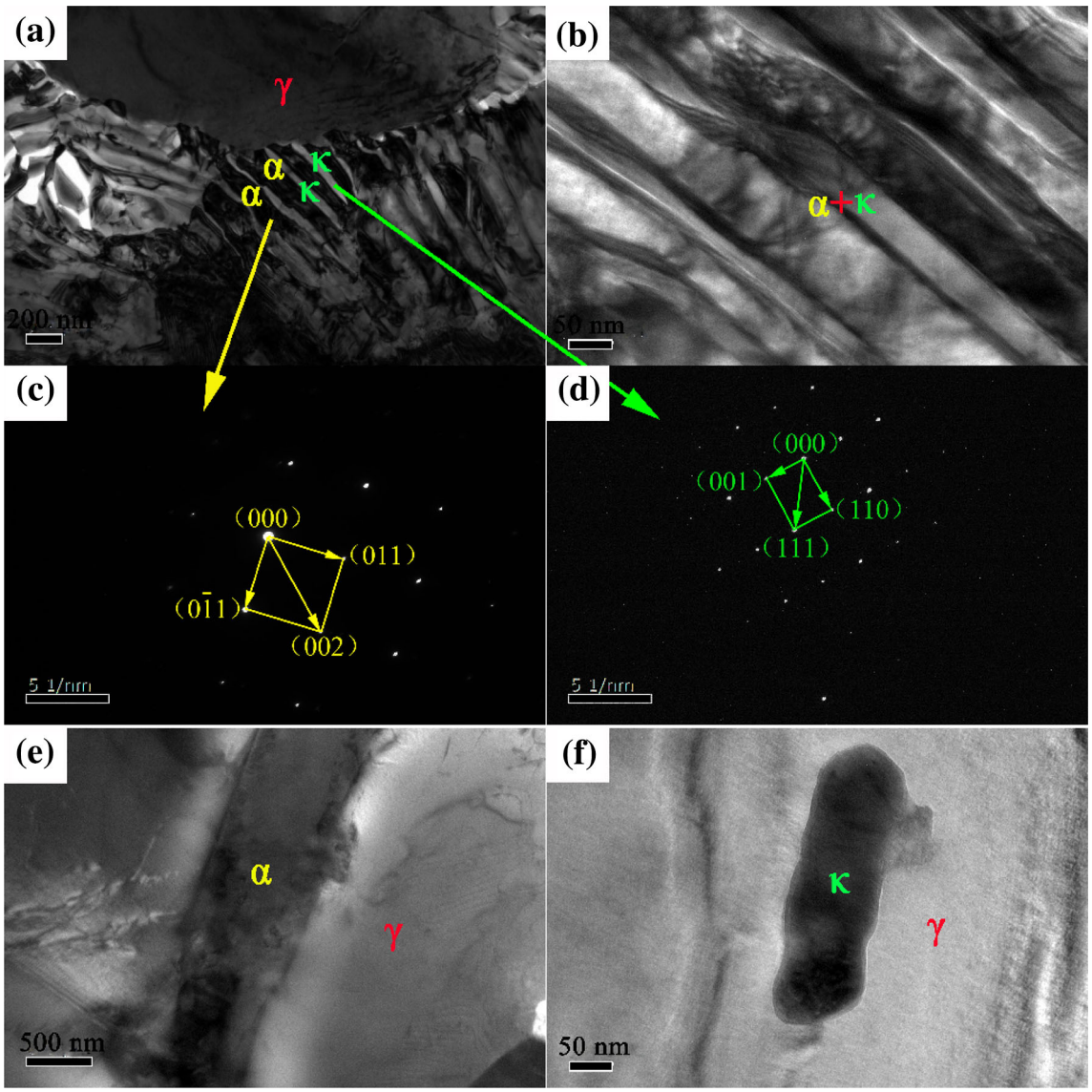

Fig. 9 TEM images of 600 °C-aged steel strip. **a** BF image; **b** magnified image of α + κ; **c** SADP along $[100]_{\alpha}$ zone axis of ferrite; **d** SADP along $[1\bar{1}0]_{\kappa}$ zone axis of κ-carbide; **e** BF image of ferrite; **f** BF image of κ-carbide

4 Conclusions

1. In the as-cast low-density Fe–12Mn–9Al–1.2C steel strip prepared under the near-rapid solidification, there were austenite and ferrite (in 27.4 vol.%) two major constituent phases, and nano-scale κ-carbides were dispersed in the austenite matrix. The ferrite was in irregular short rod or granular shapes, rather than banded microstructure reported in steels with similar composition made by traditional method involving heat treatment and hot/cold rolling. The as-cast steel strip possessed UTS of 1182 MPa and TE of 28.1%.
2. Aging treatment at 400 and 600 °C for 3 h enhanced the tensile strength and Young's modulus of the steel strip. However, when the aging temperature was above 600 °C, total elongation significantly decreased, because of a eutectoid reaction of $\gamma \rightarrow \alpha + \kappa$.
3. The strength and specific strength of the low-density Fe–12Mn–9Al–1.2C steel strip were much higher than those of low-density steels made by traditional methods with similar compositions. The highest strength and specific strength are 1393 MPa and 202.2 MPa cm^3/g for 600 °C-aged strips.
4. This work demonstrated that the near-net shape under near-rapid solidification can directly produce high-performance steel strip from liquid, which can simplify or even eliminate rolling and heat treatment procedures. It is an efficient and environmentally benign approach to fabricate the advanced low-density steels with promising mechanical properties.

Table 2 Comparison of present steel with steels prepared by traditional methods

Composition	Process	Ferrite fraction/ vol.%	Tensile properties				
			YS/ MPa	UTS/ MPa	TE/%	UTS × TE/ (GPa %)	SS/ (MPa cm^3 g^{-1})
Fe–12Mn–9Al–1.2C	Near-rapid solidification	13.3	1012	1182	28.1	33.2	171.6
Fe–12Mn–9Al–1.2C	Near-rapid solidification + aging at 400 °C for 3 h	14.6	1124	1266	30.7	38.9	183.7
Fe–12Mn–9Al–1.2C	Near-rapid solidification + aging at 600 °C for 3 h	22.7	1316	1393	12.6	17.6	202.2
Fe–12Mn–8Al–0.8C [32]	Homogenizing at 1200 °C for 2 h + hot rolling + annealing at 1000 °C for 1 h + cold rolling + annealing at 900 °C for 15 min + water quenching	30.0	670	920	46.4	42.7	130.5
Fe–10Mn–10Al–0.7C [31]	Homogenizing at 1200 °C for 1 h + hot rolling + water quenching to 300 °C + annealing at 900 °C for 1 h + water quenching	40.0	651	855	36.6	31.3	125.7

YS yield strength, *SS* specific strength

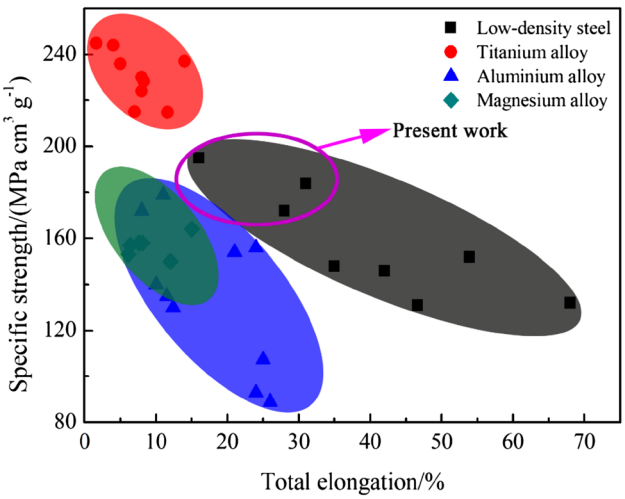

Fig. 10 Comparison of mechanical properties of investigated steels and other alloys [26, 32, 35–46]

Acknowledgements This work was financially supported by the Joint Fund of Iron and Steel Research (No. U1660103) and National Natural Science Foundation of China (No. 51574162). TEM tests were conducted in the Instrumental Analysis and Research Center at Shanghai University. The authors would like to express sincere thanks for the staff support at the Center.

References

[1] S.L. Zheng, H.H. Xu, J.Z. Feng, Z.X. Zheng, Y.T. Wang, L.L. Lu, Chin. J. Mech. Eng. 24 (2011) 1111–1115.
[2] R.A. Witik, J. Payet, V. Michaud, C. Ludwig, J.A.E. Månson, Composites, Part A 42 (2011) 1694–1709.
[3] Z. Mi, D. Tang, L. Yan, J. Guo, J. Mater. Sci. Technol. 21 (2005) 451–454.
[4] H. Helms, U. Lambrecht, Int. J. Life Cycle Assess. 12 (2007) 58–64.
[5] F. Bonnet, V. Daeschler, G. Petitgand, Can. Metall. Quart. 53 (2014) 243–252.
[6] S. Das, B.E. Tonn, J.H. Peretz, Res. Eval. 17 (2008) 133–148.
[7] D.W. Suh, N.J. Kim, Scripta Mater. 68 (2013) 337–338.
[8] S.G. Peng, R.B. Song, Z.D. Tan, C.H. Cai, K. Guo, Z.H. Wang, J. Iron Steel Res. Int. 23 (2016) 857–866.
[9] H.K.D.H. Bhadeshia, Scripta Mater. 70 (2014) 12–17.
[10] H.K.D.H. Bhadeshia, ISIJ Int. 56 (2016) 24–36.
[11] S. Kang, Y.S. Jung, J.H. Jun, Y.K. Lee, Mater. Sci. Eng. A. 527 (2010) 745–751.
[12] S. W. Hwang, J.H. Ji, K.T. Park, Mater. Sci. Eng. A. 528 (2011) 7267–7275.
[13] K.T. Park, Scripta Mater. 68 (2013) 375–379.
[14] H. Springer, D. Raabe, Acta Mater. 60 (2012) 4950–4959.
[15] I. Gutierrez-Urrutia, D. Raabe, Scripta Mater. 68 (2013) 343-347.
[16] S.S. Sohn, B.J. Lee, S. Lee, N.J. Kim, J.H. Kwak, Acta Mater. 61 (2013) 5050–5066.
[17] S.H. Wang, Z.Y. Liu, W.N. Zhang, G.D. Wang, J.L. Liu, G.F. Liang, ISIJ Int. 49 (2009) 1340–1346.
[18] M. Leonhardt, W. Löser, H.G. Lindenkreuz, Acta Mater. 47 (1999) 2961–2968.
[19] M. Leonhardt, W. Löser, H.G. Lindenkreuz, Mater. Sci. Eng. A 271 (1999) 31–37.
[20] A.A. El-Daly, A.M. Abdel-Daiem, M. Yousf, Mater. Chem. Phys. 71 (2001) 111–119.
[21] A.A. El-Daly, A.M. Abdel-Daiem, M. Yousf, Mater. Chem. Phys. 74 (2002) 43–51.
[22] A.A. El-Daly, A.M. Abdel-Daiem, M. Yousf, Mater. Chem. Phys. 78 (2003) 73–80.
[23] C.J. Song, W.B. Xia, J. Zhang, Y.Y. Guo, Q.J. Zhai, Mater. Des. 51 (2013) 262–267.
[24] C.J. Song, W. Lu, K. Xie, Y.H. Zhang, W.B. Xia, K. Han, Q.J. Zhai, Mater. Sci. Eng. A 610 (2014) 145–153.
[25] L.B. Liu, C.M. Li, Y. Yang, Z.P. Luo, C.J. Song, Q.J. Zhai, Mater. Sci. Eng. A 679 (2017) 282–291.
[26] L.F. Zhang, R.B. Song, C. Zhao, F.Q. Yang, Mater. Sci. Eng. A 640 (2015) 225–234.

[27] Z.Q. Wu, H. Ding, X.H. An, D. Han, X.Z. Liao, Mater. Sci. Eng. A 639 (2015) 187–191.
[28] W.J. Lu, X.F. Zhang, R.S. Qin, Ironmak. Steelmak. 42 (2015) 626–631.
[29] K.T. Park, S.W. Hwang, C.Y. Son, J.K. Lee, JOM 66 (2014) 1828–1836.
[30] R. Yang, W.B. Xia, C.J. Song, Q. Peng, X.Y. He, Q.J. Zhai, Adv. Mater. Res. 391-392 (2012) 741–744.
[31] C. Zhao, R.B. Song, L.F. Zhang, F.Q. Yang, T. Kang, Mater. Des. 91 (2016) 348–360.
[32] Z.Q. Wu, H. Ding, H.Y. Li, M.L. Huang, F.R. Cao, Mater. Sci. Eng. A 584 (2013) 150–155.
[33] W.K. Choo, J.H. Kim, J.C. Yoon, Acta Mater. 45 (1997) 4877–4885.
[34] R.P. Dalai, S. Das, K. Das, Can. Metall. Quart. 53 (2014) 317–325.
[35] P. Mónica, P.M. Bravo, D. Cárdenas, J. Mater. Process. Technol. 239 (2017) 297–302.
[36] E. Welsch, D. Ponge, S.M.H. Haghighat, S. Sandlöbes, P. Choi, M. Herbig, S. Zaefferer, D. Raabe, Acta Mater. 116 (2016) 188–199.
[37] X.F. Wang, M.X. Guo, L.Y. Cao, X.Y. Peng, J.S. Zhang, L.Z. Zhuang, J. Wuhan Univ. Technol. Mater. Sci. Ed. 31 (2016) 648–653.
[38] J. Shen, K.Kondoh, T.L. Jones, S.N. Mathaudhu, L.J. Kecskes, Q. Wei, Mater. Sci. Eng. A 649 (2016) 338–348.
[39] M.C. Santos, A.R. Machado, W.F. Sales, M.A.S. Barrozo, E.O. Ezugwu, Int. J. Adv. Manuf. Technol. 86 (2016) 3067–3080.
[40] B.V. Ramnath, C. Elanchezhian, M. Jaivignesh, S. Rajesh, C. Parswajinan, A.S.A. Ghias, Mater. Des. 58 (2014) 332–338.
[41] T. Dursun, C. Soutis, Mater. Des. 56 (2014) 862–871.
[42] S. Leuders, M. Thöne, A. Riemer, T. Niendorf, T. Tröster, H.A. Richard, H.J. Maier, Int. J. Fatigue 48 (2013) 300–307.
[43] G. Frommeyer, U. Brüx, Steel Res. Int. 77 (2006) 627–633.
[44] F.J. Gil, J.M. Manero, M.P. Ginebra, J.A. Planell, Mater. Sci. Eng. A 349 (2003) 150–155.
[45] P. Marmy, T. Leguey, J. Nucl. Mater. 296 (2001) 155–164.
[46] A.W. Bowen, Mater. Sci. Eng. 40 (1979) 31–47.